MECHANISMS AND MECHANICS OF DAMAGE IN COMPOSITES

D. François*

Abstract : Even for very old composites materials such as bricks or concrete, not to speak of young modern composite materials, the damage behaviour needs to be better understood. It is a multiscale phenomenon. Roughly speaking the fracture resistance is given by the law of mixture when the more brittle element fails. Except for concrete, the best specific fracture resistance would be achieved by the highest possible volume fraction of reinforcement. The model of Kelly provides a good insight in the damage of unidirectional fiber reinforced composites either by fiber or by interface fracture. Axisymmetrical finite element modelling allows to more precisely understand which type is prefered. The influence of an interphase is important. Local fluctuations in the volume fraction or in the alignment of fibers play an essential role. The initiation of damage at particles reinforcements can be predicted using models derived from Eshelby's inclusion. The probability of failure of a volume element can be deduced from the distribution of microstructural elements. Examples are given for Al C composite, an adhesive and a SMC.

key words : composites, fiber reinforcement, particles reinforcement, damage, micromechanics, adhesive.

* École Centrale de Paris, CNRS URA 850, Grande voie des vignes, F-92295 Châtenay-Malabry Cedex

INTRODUCTION

Composite materials for structural applications are designed to combine different desirable properties so as to improve the mechanical behaviour. Two main characteristics are wanted, good fracture resistance and good stiffness, often independently. Professor Mori drew my attention on the first recorded example of a composite material (1). When the pharaoh was complaining about the bad comportement of the Jews he deprived them of straw for the fabrication of the numerous bricks they were forced to manufacture. They then had to glean in order to obtain the fibers needed to consolidate clay. This is a case where the material working essentially in compression, a better stiffness is not the objective, but the fracture resistance must be improved. Concrete is another such example, the particulates preventing easy cracking of the cement paste, as the Romans had so well mastered. Much later only was the amelioration of stiffness sought. Polymers offered attractive properties but lacked rigidity and it was discovered to be feasible to incorporate glass fibers to build hulls for instance. Space developments with the need for high specific properties were decisive in promoting composites for both purposes : stiffness and resistance.

Except for crude bricks and concrete, composite materials are so much younger than steels and cupper alloys, that in spite of a wealth of research, their mechanical properties are not perfectly mastered. Designers do not have the same feeling for the use of these materials as their instinctive dimensionning of much manipulated traditional alloys. Norms, codes, rules are lacking to a large extend. The properties often display a large scatter. I was once called to a textile factory which was lockouted because the septic tank, made of fiber glass reinforced polymer, had failed under the weight of soil. Such stupid accidents are avoidable but progress is certainly needed in the understanding of the mechanical behaviour of composites. Attempting a complete review of the present knowledge would be preposterous. I will simply try to show how a better comprehensibility of fracture resistance was achieved on a few examples mostly taken from my laboratory.

A better knowledge about this property needs a close scrutiny of the fracture mechanisms. For composite materials the scale at which the phenomena are observed is essential. Looked from far away the material is homogeneous. It reveals its heterogeneous nature under closer examination. It can then be treated as a structure made of two materials. Often a still larger magnification discloses new heterogeneities, and so on. Concrete offers a good example of this need to go through a large span of scales, from the microscopic platelets of hydrated carbonates and silicates in the cement paste, to the mesoscopic gravels of the mortar, the macroscopic stones in the concrete and finaly even to the steel reinforcements in constructions. The damage develops gradually at these different scales and it is the very reason for its

resistance to crack propagation.

Indeed the improvement of the fracture toughness brought about by the incorparation of particles or fibers, comes from either the stabilization of micro cracks and consequently of their multiplication or from preventing crack opening by bridging. In the cases where theses mechanisms do not operate the fracture toughness can be very low as it is the case in metallic matrix composites.

Composite materials can be roughly classified in two categories. Those which are reinforced by fibers and those which are reinforced by particles. The fracture processes and their modelizations are somewhat different for those two categories and will be treated separately. I will first deal with the initiation of damage and secondly with the propagation of cracks.

FRACTURE OF FIBER REINFORCED COMPOSITES

To a first approximation the stress in the direction of the fibers when they are aligned is the volumetric average of the stresses in the matrix and in the composite. Damage initiation occurs when the most brittle constituent fails. When the fibers are the more brittle, the fracture stress σ_R of the composite is given by

$$\sigma_R = vR_f + (1-v)\sigma_m(\frac{R_f}{E_f})$$

where v is the volume fraction of fibers, R_f their fracture resistance and $\sigma_m(\frac{R_f}{E_f})$ the stress in the matrix when the deformation is equal to the fracture strain of the fibers $\epsilon_f = R_f/E_f$, E_f being their Young's modulus. A similar expression could be written for a composite made of a matrix more brittle then the fibers. In many applications a high **specific resistance** is sought : for a piece loaded in tension the ratio σ_R/ρ must be as high as possible, ρ being the density. For a plate working in bending the optimizing ratio is $\sigma_R^{1/2}/\rho$ (2). As the density of the composite is the volume average of the densities of the constituants, it might turn out that an optimum volume fraction would exist. Simple calculations show that for the ratio σ_R/ρ as high a volume fration as possible is the answer. However a maximum of the ratio $\sigma_R^{1/2}/\rho$ appears for a volume fration v_{opt} given by

$$v_{\text{opt}} = \frac{1}{f_f/\rho_m - 1} - \frac{2}{R_f/\sigma_m(\epsilon_f) - 1}$$

where ρ_f and ρ_m are the densities of the fibers and of the matrix respectively. Figure 1 shows that for a certain combination of properties such an optimum volume fraction exists. However most composites are such that they fall in the area under the curve corresponding to $v_{\text{opt}} = 1$ in which case as many

fibers as possible should be incorporated. Reinforced concrete looks like a case where an optimum steel volume fraction of about 0.25 might be desirable for plates in bending. A similar consideration could be used for the buckling of columns the ratio R_f/σ_m being replaced by the ratio E_f/E_m of Young's moduli. I will not deal further with compressive loading of fibers reinforced composites, in spite of the fact that their resistance to compression is one of their most critical weakness, and one which has not deserved enough research.

A better insight of the behaviour of fiber reinforced composites is given by the **model of Kelly** (3). I recall that this model is based on the equilibrium of a thin slice of a fiber to which the load is transfered by shear at the interface (figure 2a)

$$2\pi r_f \tau + \pi r_f^2 \frac{d\sigma_f}{dx} = 0$$

where r_f is the radius of the fiber, τ the shear stress at the interfaces, σ_f the normal stress in the fiber.

When the matrix and the fiber remain elastic, τ exhibits a hyperbolic sine variation, being maximum at both ends of the fiber, while σ_f exhibits a hyperbolic cosine variation whith the maximum at the center of the fiber length (figure 2b).

In the case of a plastic matrix the yield limit k is first reached at both ends of the fiber at the interface, and after full plastification the normal stress distribution in the fiber is linear with a maximum at the center equal to

$$\sigma_{f\max} = k\frac{l}{r_f}$$

where k is the constant yield stress in shear ($k = \sigma_y/2$ for the Tresca criterion), l the length of the fiber (figure 2c). The fiber breaks when $\sigma_{f\max}$ reaches the fracture resistance R_f. Thus those fibers shorter than $r_f R_f/k$ do not break and the fibers breaking gives pieces whose average length is given by this same expression (figure 3).

The length of the fibers debris is in fact statistically distributed because the fibers contains a statistical distribution of defects. Assuming a Weibull distribution of the fracture resistance R_f of the fibers i.e :

$$\mathrm{Ln}\,\frac{1}{1-P_R} = \left(\frac{\sigma}{\sigma_u}\right)^m \cdot \frac{V}{V_0}$$

where m and $V_0\sigma_u^m$ are the Weibull parameters, V the volume and P_R the fracture probability, as the stress variation in the fibers is linear

$$\mathrm{Ln}\,\frac{1}{1-P_R} = 2\int_0^{l/2} \frac{\pi r_f^2}{\sigma_u^m V_0}\left(\frac{2k}{r_f}\right)^m x^m dx = \left(\frac{\pi}{m+1}\right)\left(\frac{l^{m+1}}{r_f^{m-2}V_0}\right)\left(\frac{k}{\sigma_u}\right)^m$$

As m is usually rather large the size distribution of l should not be too wide and the average not very different from the above value.

In certain cases the loading at the interface is not by plastic yielding but by friction of the matrix on the fiber (4,5,6).

The shear stress is then equal to $\mu\sigma_r$, μ being the friction coefficient and σ_r the radial stress at the interface. This stress is due to the Poisson shrinkage of the matrix and furthermore to the shrink fit residual stress σ_{rt} arising from the difference of the thermal expansion coefficients of the matrix and the fibers. The increased magnitude of the interface shear stress at both ends of the fibers can break the interface itself. Thus at the fibers end exist a fracture zone and a sticking zone. A good correlation can be found between the maximum length of the fibers which stick out of the fracture surface (figure 4) and the calculated length of the broken interface.

$$l_c = \frac{E_f\epsilon - 2\tau_R/n}{2\mu(\nu_m E_m \epsilon - \sigma_{rt})}$$

where τ_R is the shear fracture stress of the interface and

$$n = \left[\frac{E_m}{E_f(1+\nu_m)\mathrm{Ln}\,(R/r_f)}\right]^{1/2}$$

R being the distance between fibers (5,6).

In a composite whose characteristics were E_f = 75 000 MPa, E_m=3450 MPa, ν_m=0.35, ν_f=0.50, r_f=6 μm, R=16 μm, μ=0.2, σ_{rt}=-30 MPa, τ_R =50 MPa, the length l_c was found to be equal to 330 μm at the fracture stress of the composite 920 MPa.

The same model can also be used for a broken bundle of fibers (5,6) whose Young's modulus is calculated from the volume fraction of fibers in the bundle. It is then found that the shear stress at the interface as well as the broken length l_c increase as the radius of the broken bundle increases.

The preceding models do not allow to calculate the stresses induced in the neighbouring fibers by the fracture of one of them or of a bundle of fibers. A **finite element computation** gave some interesting results in the case of an epoxy resin reinforced by glass fibers (5,6). The axisymmetric cell which was considered included a central fiber surrounded by successive cylindrical layers representing the matrix and the neighbouring fibers and the whole being enclosed in a cylinder of an homogeneous material equivalent to the composite (figure 5). When the central fiber is broken two types of stress concentration appear : normal stress concentration in the adjacent layer and shear stress concentration at the neighbouring interface. Two types of fracture can then be produced : fracture of the fibers inducing a mode I crack propagation ; shear fracture of the interfaces inducing a mode II crack

propagation along the fibers. It was found that these two types of stress concentrations did not follow the same trend when the volume fraction of fibers was increased (figure 6). The normal stress concentration increases whereas the shear stress concentration at the interface would decrease a little. This explains that the zones which contain a large volume fraction of fibers break perpendicularly to the axial load and that, on the contrary, those which contain a low volume fraction of fibers exhibit fiber delamination. This is evidenced on the fractography shown on figure 4.

Furthermore when the crack propagates from one fiber to the next ones, the same kind of calculation showed that the shear stress concentration increased more rapidly than the normal stress concentration. This explains why in such composites the fracture which starts by a mode I propagation accross a bundle of fibers, at one time shifts to a delamination along the fibers (figure 7).

Another approach to a similar problem was to compute the strain energy release rate G for an annular crack by an axisymmetric finite element model. This case under study was that of a SiC-SiC composite in which the matrix is more brittle than the fibers (7). Figures 8a,b demonstrate the role of an "interphace". G_I is for a crack in mode I, $G_i(M/I)$ for a crack propagation along the interface between the matrix and the interphase and $G_i(I/F)$ between the interphase and the fiber. A soft interphase (figure 8a) favors the propagation along the interface between the matrix and the interphase. A rigid interphase on the contrary (figure 8b) creates a much larger strain energy release rate for the fracture of the fiber, and, were the toughness of the interface low enough, it is along the fiber that the propagation would take place.

These models emphasize the **importance of the local distribution of fibers** on the damage, whereas it hardly modifies the elastic properties. Another kind of local defects is the misalignment of fibers. This was again studied (5,6) by the finite element axisymmetric model in which some fibers were misoriented (figure 9) resulting in a decreasing normal stress concentration when the misorientation angle increases. Would all the fibers be perfectly aligned they would break at a stress level which is larger than the one attained when a few fibers only are perfectly aligned thus carrying most of the load. Some distributions of misalignment are thus more favorable than others (figure 10).

FRACTURE OF PARTICLES REINFORCED COMPOSITE

I include in this category the composites containing short fibers which can be considered as elongated inclusions. In those composites stress concentrations are created at the particles and the damage initiates either at the interface of in the particles (figure 11). The residual stresses due to shrink fit from

the difference of the thermal expansion coefficients of the particles and the matrix play an important role. Indeed in many instances it seems that there is no other bonding between the particles and the matrix.

The model of Mori and Tanaka (8) derived from Eshelby's inclusion theory (2) allows to calculate those shrink fit stresses as well as the ones which are added when the composite is loaded, taking into account the local fluctuations of volume fraction, size, aspect ratio and orientation of the particles.

The model (10,11) consists of three phases. The first one is the **representation** which yields a quantitative description of the microstructure. The second one is the **localization** which is the calculation of the local stresses at the particles. The third one is the **homogenization** which yields the macroscopic relation between the stress and the strain tensors. The calculation is carried out on an elementary representative volume (ERV), containing enough particles to be considered as homogeneous. A macroscopic stress tensor $\boldsymbol{\Sigma}$ is applied on this ERV. A macroscopic strain tensor $\boldsymbol{E}$ results. Locally within the ERV the stress fluctuates and is thus given by $\boldsymbol{\Sigma} + \boldsymbol{\sigma}$ the volume average of $\boldsymbol{\sigma}$ being zero. Let $\boldsymbol{E}_0 = \boldsymbol{C}_m^{-1}\boldsymbol{\Sigma}$ and $\overline{\boldsymbol{E}} = \boldsymbol{C}_m^{-1} < \overset{m}{\boldsymbol{\sigma}} >_{D-\Omega}$ where $\boldsymbol{C}_m$ is the tensor of elastic stiffness coefficients of the matrix material, $< \overset{m}{\boldsymbol{\sigma}} >_{D-\Omega}$ is the average of $\boldsymbol{\sigma}$ over the volume $D-\Omega$ of the matrix excluding the particles:

A particle is now introduced in the deformation field $\boldsymbol{E}_0 + \overline{\boldsymbol{E}}$. The local stress-strain relation yields

$$\boldsymbol{\Sigma} + \boldsymbol{\sigma} = \boldsymbol{C}_f(\boldsymbol{E}_0 + \overline{\boldsymbol{E}} + \boldsymbol{e})$$

where $\boldsymbol{e}$ is the deformation induced by that particle, whereas $\boldsymbol{\sigma}$ results from all particles. $\boldsymbol{C}_f$ is the tensor of elastic stiffness coefficients of the particle.

This particle is now transformed in an equivalent inclusion with the elastic properties of the matrix material, but submitted to an extra strain $\boldsymbol{e}^*$. It is related to $\boldsymbol{e}$ by Eshelby's tensor $\boldsymbol{s}$

$$\boldsymbol{e} = \boldsymbol{s}\boldsymbol{e}^*$$

This tensor depends upon the shape of the inclusion and the elastic constants.

Now

$$\boldsymbol{\Sigma} + \boldsymbol{\sigma} = \boldsymbol{C}_m(\boldsymbol{E}_0 + \overline{\boldsymbol{E}} + \boldsymbol{e} - \boldsymbol{e}^*)$$

which can be equated with the above relation for $\boldsymbol{\Sigma} + \boldsymbol{\sigma}$. This gives the localization relation

$$\begin{aligned}\boldsymbol{e}^* &= \left[(\boldsymbol{C}_m - \boldsymbol{C}_f)(\boldsymbol{s} - \boldsymbol{I}) - \boldsymbol{C}_f\right]^{-1}(\boldsymbol{C}_f - \boldsymbol{C}_m)(\boldsymbol{E}_0 + \overline{\boldsymbol{E}}) \\ &= \boldsymbol{Q}(\boldsymbol{E}_0 + \overline{\boldsymbol{E}})\end{aligned}$$

$\boldsymbol{Q}$ being the localization tensor, which is completely known.

σ must now be calculated. It comes out by homogenization the average value of σ over the whole volume D, including the particles, being equal to zero.

As this model, based on Eshelby's inclusion isolated in an infinite medium, neglects the interaction with other particles, a complementary element in the localization tensor Q was included. To the free strain e^* was added a free strain δ^* coming from the local fluctuations of the volume fraction v_i of particles.

$$\delta^* = e^*(v_i) - e^*(v)$$

v is the average volume fraction with

$$e^*(v_i) = LE_0 \qquad \text{and} \quad e^*(v) = L_0 E_0$$

This model allows first of all to calculate the **shrink fit stress** which is developed during cooling. Figure 12 shows the evolution of the translation vector of the yield surface for an Al C composite due to those residual stresses as a function of the aspect ratio of the short C fibers. The effect is much more important in the axial direction of the fibers. It shows that the Al matrix is loaded in tension in this direction as the C fibers expand during cooling.

As the model yields the stresses in the inclusion and at the interface it can be used to determine the **initiation of damage** under a certain complex stress system. In the case of the Al C composite (12,13) it was assumed that this initiation began when the local interface stress due to the applied load compensated the radial compressive residual stress. Figure 13 shows the damage locus which can be calculated in the stress space. In this case it is well inside the yield surface explaining the very early damage initiation in MMC.

This model allows also to calculate the **damage probability** taking into account the distribution of the local volume fraction, as the stress at the interface is larger when the neighbouring inclusions are closer. Figure 14 shows a comparison between the experimental fracture probability and the probability of damage initiation calculated from the distribution of the local volume fraction determined by image analysis (figure 15). Part of the difference must be due to the influence of the orientation of the fibers which is not included in the analysis. It must be noted also that damage initiation precedes fracture and that a mean for its detection was lacking. Nonetheless a fair agreement is observed at low probabilities. Figure 16 points again to the great importance of local microstructural fluctuations for damage initiation, as with the same total volume fraction of short carbon fibers in aluminium, two different distributions lead to large differences in the failure probability.

Two other examples illustrate the use of this model. In adhesive joints very high hydrostatic tensile stresses can be created. Figure 17 shows how, in

these conditions, microscopic cracks develop at the interface of elastomeric inclusions in the epoxy matrix of the adhesive (14). From the knowledge of the elastic properties of both constituents (E_m=2200 MPa, ν_m=0.36, E_F=100 MPa, ν_f=0.49, v=8.5%), it was possible to derive the damage initiation criterion using Eshelby's tensor for a sphere

$$s_{iiii} = \frac{7 - 5\nu_m}{15(1 - \nu_m)} \quad s_{iijj} = \frac{5\nu_m - 1}{15(1 - \nu_m)} \quad s_{ijij} = \frac{4 - 5\nu_m}{15(1 - \nu_m)}$$

The damage criterion is the following :

$$\Sigma_1 = 4.23\sigma_c - 3.23\Sigma_H$$

where Σ_1 is the maximum principal stress, Σ_H the hydrostatic stress and σ_c the fracture stress of the inclusion interface.

The initiation of damage was studied in a SMC composite material made of a polymeric matrix reinforced with randomly oriented fibers (15). The elastic behaviour of the polyester matrix in that case depended on the incorporation of $CaCO_3$ small particles, which are visible at a lower scale than the fibers. In this interesting example of a multiscale material the model was applied in two steps. The first one allows to compute the elastic stiffness coefficients of the matrix and the second one the macroscopic elastic properties of the composite including the fibers (figure 18). The effect of damage on these properties can also be evaluated by replacing the decohered fibers by a fictitious softer inclusion.

CONCLUSION

Damage in composites is a multiscale phenomenon. Simple analytical models were developed for fibers or for particles which allow to calculate the initiation of damage and especially to evaluate the effects of microsctructural fluctuations of the local volume fraction, of the orientation, shapes and size of the particles. All these which do not influence so much the elastic properties, play a very important role in the development of damage. Axisymmetric finite element models were also used to study more precisely cracking at the scale of fibers or particles. The stength of the interface is a very important parameter and more experiments should be devised to measure this strength as well as that of interphases which can modify greatly the damage behaviour of composites.

SYMBOLS USED

C_m = tensor of the stiffness coefficients of the matrix

C_f = tensor of the stiffness coefficients of the particles

D = volume of the representative elementary volume

e = strain tensor induced by an inclusion

e^* = free strain tensor of an inclusion

E = macroscopic strain tensor

E_0 = average strain tensor

$\overline{E}$ = average strain tensor corresponding to the stress fluctuation in the matrix

E = Young's modulus of the composite (MPa)

E_m = Young's modulus of the matrix (MPa)

E_f = Young's modulus of the reinforcement (MPa)

G_I = strain energy release rate for mode I (N/m)

G_i = strain energy release rate for interface fracture (N/m)

k = yield stress in shear (MPa)

l = fiber length

l_c = length of the broken fiber interface

m = Weibull exponent

P_R = failure probability

Q = localization tensor

r_f = fiber radius

R = distance between fibers

R_f = fracture strength of the fibers

s = Eshelby's tensor

v = volume fraction of reinforcement

v_{opt} = optimum volume fraction

v_i = local volume fraction

V_0 = Weibull parameter

δ = interaction free strain tensor

ϵ = strain along the fibers

ϵ_f = fracture strain of the fibers

μ = friction coefficient

ν_m = Poisson ratio of the matrix

ν_f = Poisson ratio of the reinforcement

Ω = volume of the inclusions

ρ = density

ρ_m = matrix density

ρ_f = fibers density

$\boldsymbol{\sigma}$ = fluctuation of the stress tensor

σ_R = fracture stress of the composite

σ_m = stress in the fibers

σ_y = yield stress (MPa)

σ_u = Weibull parameter

σ_{rt} = fit shrink stress

σ_c = debonding stress

$\boldsymbol{\Sigma}$ = macroscopic stress tensor

Σ_H = hydrostatic stress

Σ_1 = maximum principal stress

τ = shear stress

τ_R = shear fracture stress (MPa)

REFERENCES

(1) The Holy Bible. Exodus 5

(2) Ashby, M.F., "Materials Selection in Conceptual Design", Mat. Science and Tech. 5 (1989) 517-525

(3) Kelly, A., and Davies, G.J., "The Principles of the Fibre Reinforced Metals", Metall. Rev. 10 (1965)

(4) Pigott, M.R., "Load Bearing Fiber Composites"Un. of Toronto (1980)

(5) Wang, S.J., "Étude de l'endommagement d'un composite unidirectionnel fibres de verre-matrice epoxy", Thèse de l'École Centrale de Paris (9 juillet 1990)

(6) Wang, S.J., Bompard, Ph., Baptiste, D., François, D., "Microscopic Failure Mechanisms of an Unidirectional Glass Fibre Reinforced Composite" in Mechanics and Mechanisms of Damage in Composites and Multimaterials. D. Baptiste ed. ESIS II. M.E.P. London (1991) 3-15

(7) Piquenot, N., "Étude du rôle des interfaces et interphase dans le comportement à la rupture de microcomposites unidirectionnels à matrice fragile". Thèse de l'Université de Bordeaux I (21 février 1992)

(8) Mori, T. and Tanaka, K., "Average Stress in Matrix and Average Elastic Energy of Materials with Misfitting Inclusions" Acta. Met. 21 (1973) 571-574

(9) Eshelby, J.D., "The Determination of the Elastic Field of an Ellipsoidal Inclusion and Related Problems" Proc. Roy. Soc. Series A 241 (1957) 376-396

(10) Bréban, Ph., "Composites aluminium-fibres de carbone obtenus par filage", Thèse de l'École Centrale de Paris (6 juin 1990)

(11) Baptiste, D., "Modélisation micromécanique de l'endommagement des composites", Habilitation de l'Université Paris VI (26 mars 1991)

(12) Bréban, Ph., Baptiste, D., François, D., "Damage Micromechanics Approaches to Metal Matrix Composites" J. of Adv. Science 3 (1991)

(13) Bréban, Ph., Bompard, Ph., Baptiste, D., "Influence of the Distribution of Fibers on the Properties of a coextruded Gr/Al Composite", Archives of Met. 35 (1990) and in Mechanics and Mechanisms of Damage in Composites and Multimaterials, D. Baptiste ed. ESIS II. M.E.P. London (1991)

(14) Hu, G.K., "Étude théorique et expérimentale du comportement, de l'endommagement et de la rupture des assemblages collés", Thèse de l'École Centrale de Paris (19 décembre 1991)

(15) Keyvani, M., Thèse de l'École Centrale de Paris (to be defended)

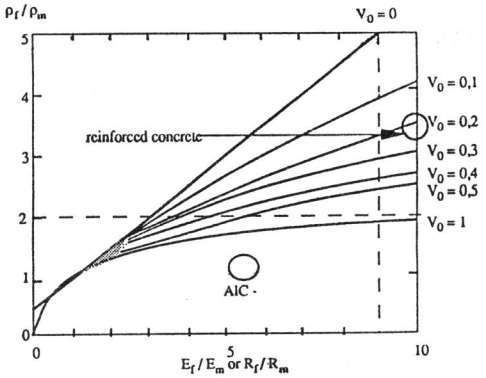

Figure 1 Volume fraction of fibers to obtain the maximum value of $R_f^{1/2}/\rho$ for optimizing the resistance of a plate in bending.

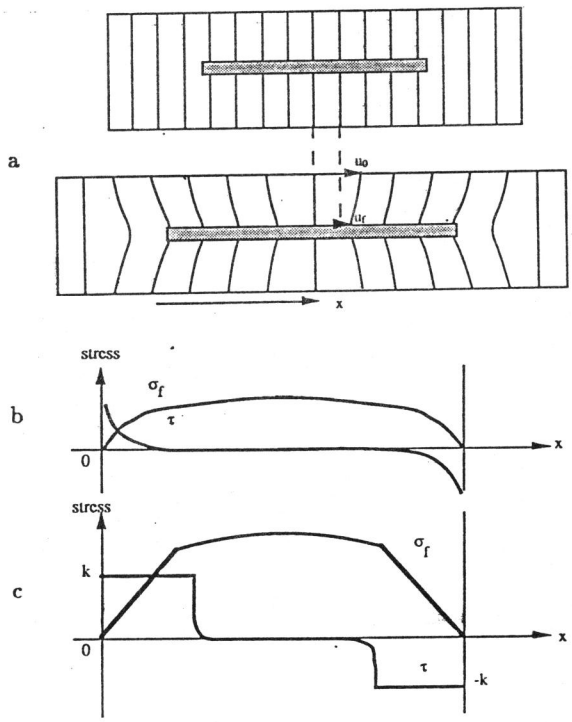

Figure 2 Load transfer on fibers (3)
2a equilibrium model, 2b elastic behaviour, 2c plastic behaviour

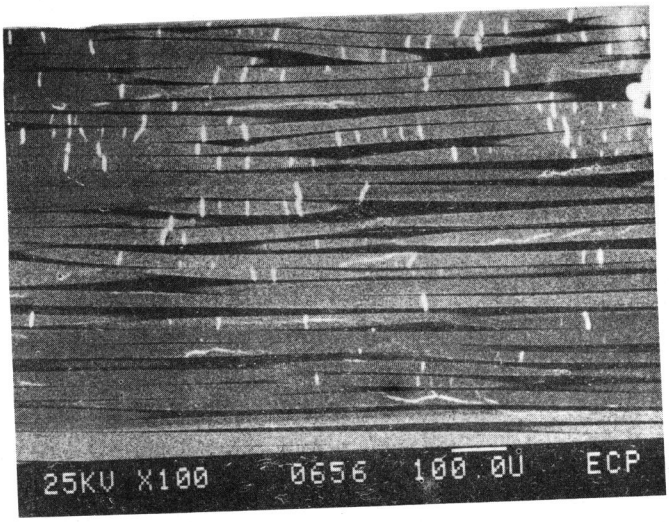

Figure 3 Micrograph showing broken fibers

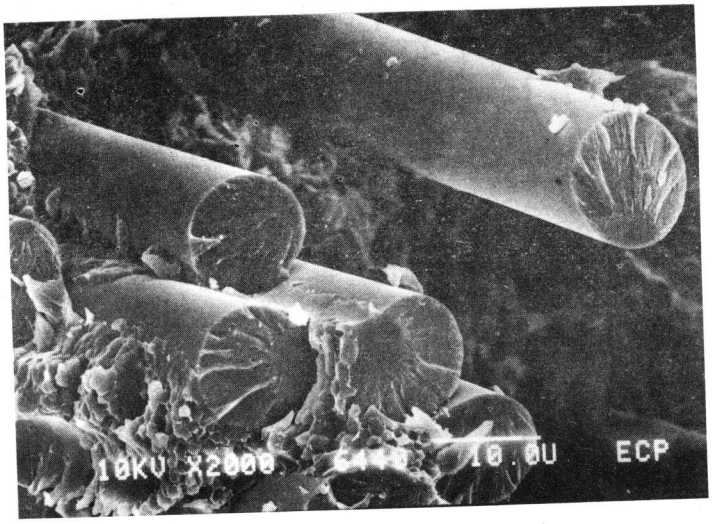

Figure 4 Fibers sticking out of the fracture surface (5)

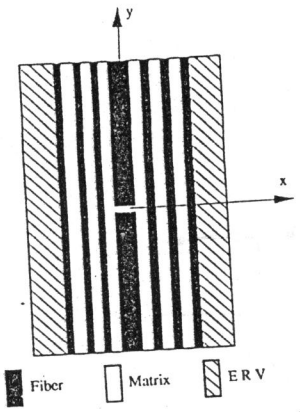

Figure 5 Finite element model for the computation of stresses produced by the fracture fibers

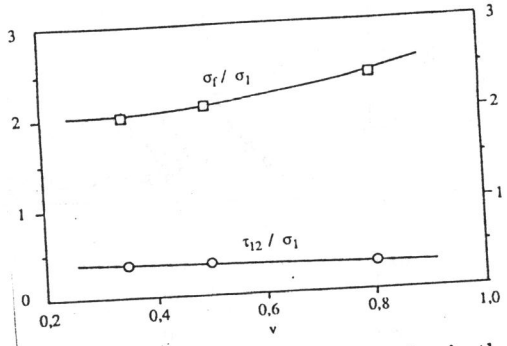

Figure 6 Normal stress concentration in the fibers and shear stress concentration at the interface as a function of the fiber volume fraction (5)

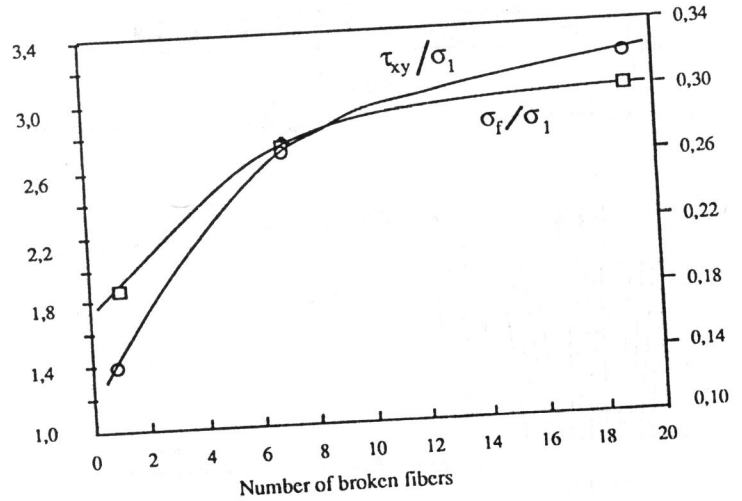

Figure 7 Normal stress concentration in the fibers and shear stress concentration at the interfaces as a function of the number of broken fibers (5)

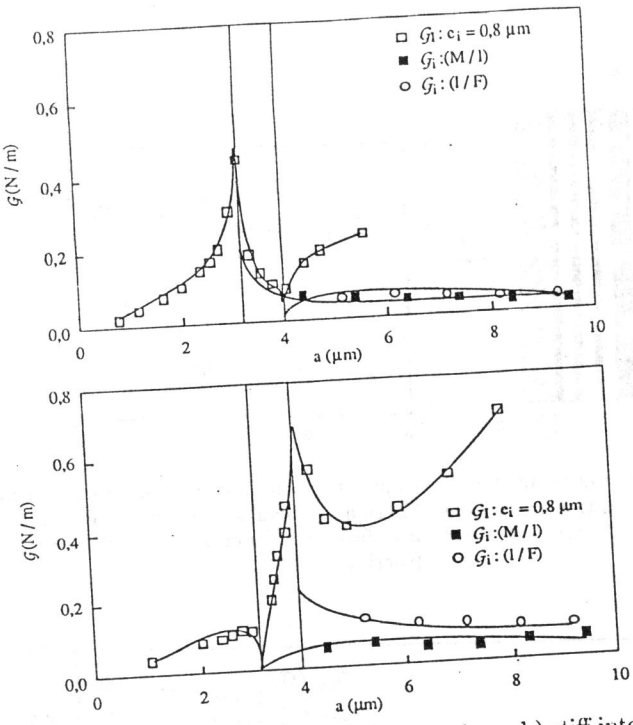

Figure 8 Strain energy release rates a) soft interphase, b) stiff interphase

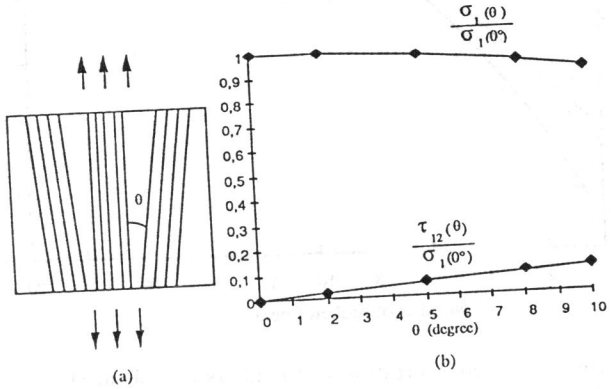

Figure 9 Normal stress concentration in the fibers and shear stress concentration at the interfaces as a function of the misorientation angle

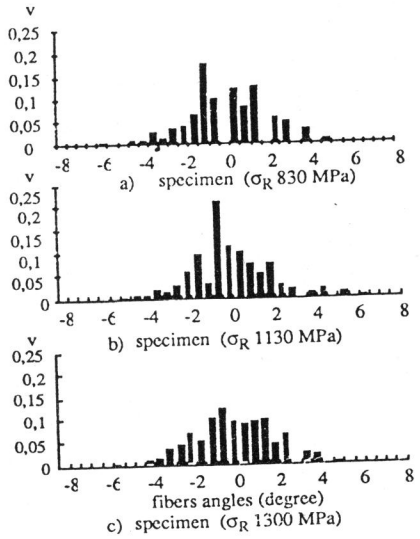

Figure 10 Influence of the misalignement distribution on the fracture resistance. Calculated stress concentration A : 1.053, B : 1.040, C : 1.030

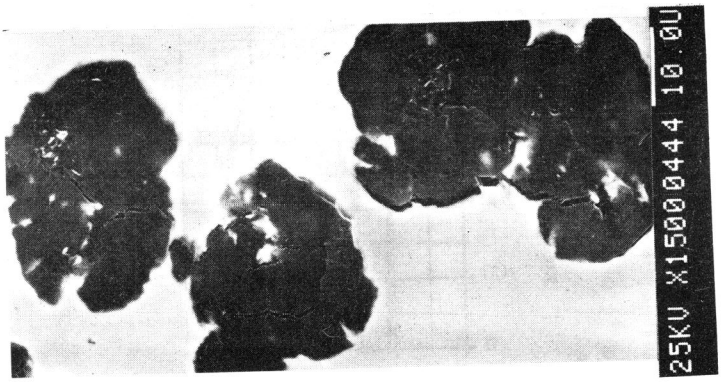

Figure 11 Damage initiation in spheroïdal graphites in cast iron (Ming Dong ECP)

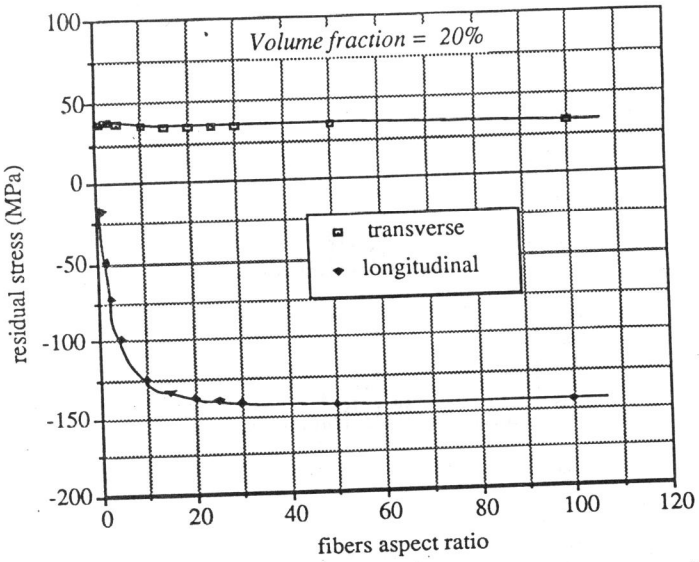

Figure 12 Translation vector of the yield surface of an C.Al composite due to cooling residual stresses as a function of the C fibers aspect ratio (10)

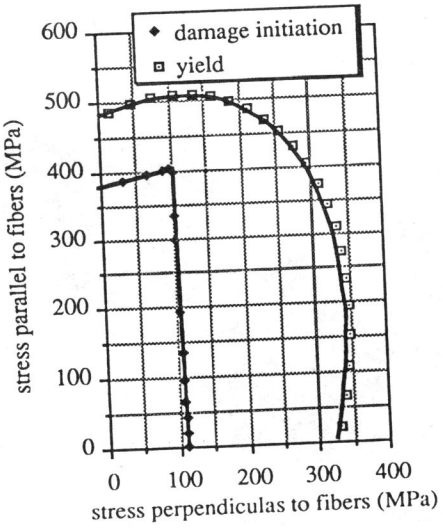

Figure 13 Damage locus in the stress space compared with the yield surface for a C.Al composite (10)

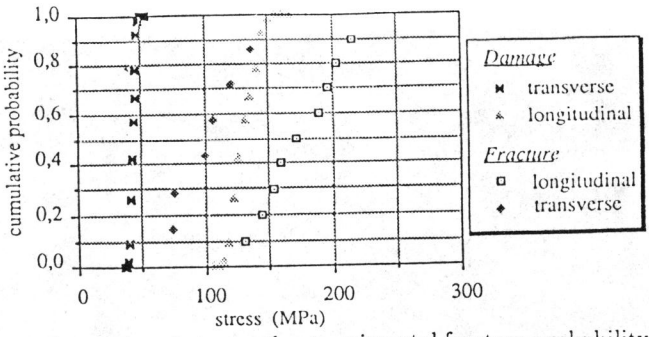

Figure 14 Comparison between the experimental fracture probability and the probability calculated from the local volume fraction (10) (see figure 15)

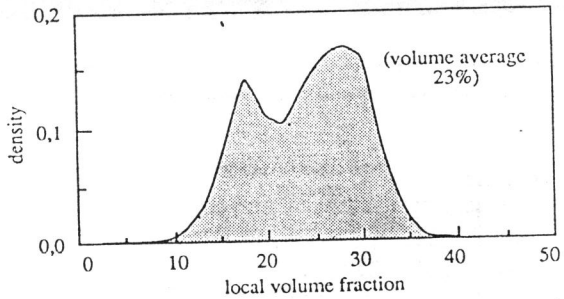

Figure 15 Distribution of the local volume fraction measured by image analysis in a C.Al composite (10)

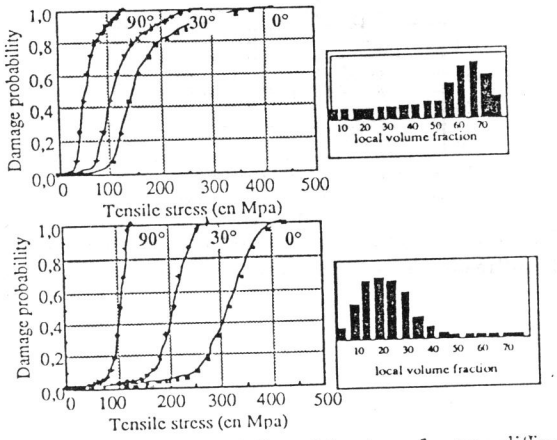

Figure 16 Evolution of the probability of fracture for two different distributions of the same total volume fraction of C in a C.Al composite (10)

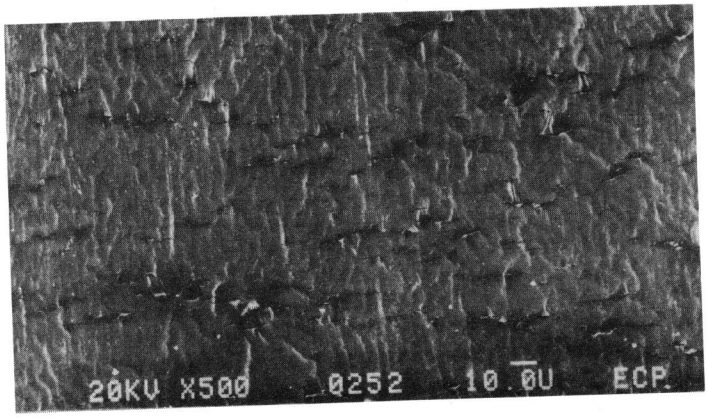

Figure 17 Micrograph showing the initiation of damage at the interface of spherical elastomere particles in an epoxy adhesive (14)

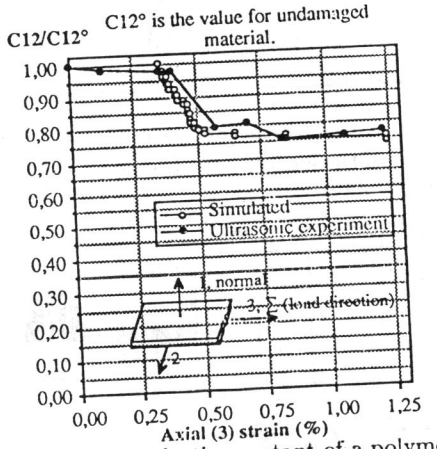

Figure 18 Evolution of the elastic constant of a polymeric matrix composite measured by ultrasounds and calculated as a function of the applied strain (15)